

The products of primary magma fragmentation finally revealed by pumice agglomerates

Thomas Giachetti^{1*}, Kathleen R. Trafton¹, Joshua Wiejaczka¹, James E. Gardner², James M. Watkins¹, Thomas Shea³ and Heather M.N. Wright⁴

¹Department of Earth Sciences, University of Oregon, Eugene, Oregon 97403, USA

²Jackson School of Geosciences, University of Texas at Austin, Austin, Texas 78712, USA

³Department of Geology and Geophysics, University of Hawaii at Manoa, Honolulu, Hawaii 96822, USA

⁴U.S. Geological Survey, Volcano Disaster Assistance Program, Vancouver, Washington 98683-9589, USA

ABSTRACT

Following rapid decompression in the conduit of a volcano, magma breaks into ash-to block-sized fragments, powering explosive sub-Plinian and Plinian eruptions that may generate destructive pyroclastic falls and flows. It is thus crucial to assess how magma breaks up into fragments. This task is difficult, however, because of the subterranean nature of the entire process and because the original size of pristine fragments is modified by secondary fragmentation and expansion. New textural observations of sub-Plinian and Plinian pumice lapilli reveal that some primary products of magma fragmentation survive by sintering together within seconds of magma break-up. Their size distributions reflect the energetics of fragmentation, consistent with products of rapid decompression experiments. Pumice aggregates thus offer a unique window into the previously inaccessible primary fragmentation process and could be used to determine the potential energy of fragmentation.

INTRODUCTION

Explosive volcanic eruptions of silicic magmas result from fragmentation of magma below Earth's surface into pyroclasts ranging in size from ash to lapilli and blocks. During magma ascent, decreasing pressure forces gas-saturated magma to nucleate bubbles of supercritical fluid. Bubbles then grow by the diffusion of volatiles from the melt and the expansion of the exsolved vapor phase, causing an increase in magma porosity, magma acceleration, and further degassing. Simultaneously, as viscous stresses in the melt impede bubble growth, vapor overpressure therein increases (Gonnermann and Manga, 2007). When bubble overpressure exceeds the tensile strength of the surrounding melt and/or if the expanding melt is subjected to a critical strain rate (Dingwell, 1996; Papale, 1999; Zhang, 1999), magma explosively fragments into pyroclasts that range from submicron (ash) to macroscale (blocks) in size.

Fall deposits from explosive Plinian eruptions of silicic magmas have a size distribution different from that expected for a single fragmentation event (Kaminski and Jaupart, 1998). The size distribution of the products of rock fragmentation invariably follows a power law, $N = \lambda d^{-D}$, where N is the number of particles greater than size d , λ is a scaling factor, and D is the power-law exponent (fractal dimension). For a variety of experimentally fragmented geological objects, fractal dimensions are always <3 and, in most cases, in the range 2.5 ± 0.3 (Turcotte, 1997; Kaminski and Jaupart, 1998). By contrast, fall deposits of silicic Plinian eruptions have total grain-size distributions that follow a power-law distribution with fractal dimension >3 ($D = 3.4 \pm 0.3$; Kaminski and Jaupart, 1998; Rust and Cashman, 2011; Pioli et al., 2019; Carazzo et al., 2020). The difference in D values between experimental and natural fragmentation products has been explained by secondary pyroclast fragmentation in response to thermal stresses during decompression and/or disruptive inter-particle collisions and abrasion

in the conduit and volcanic plume (Dufek et al., 2012; Jones et al., 2017). This D -value differential is at present an unconstrained metric of secondary fragmentation: as the true size distribution of primarily fragmented pyroclasts remains unknown, so too does the degree to which secondary fragmentation impacts pyroclast size and shape distributions. However, new textural observations of sub-Plinian and Plinian lapilli reported here, interpreted in light of recent studies into the origin of obsidian pyroclasts (Gardner et al., 2017; Watkins et al., 2017), indicate that some pumice pyroclasts form by post-fragmentation amalgamation of "protopyroclasts" prior to secondary collisional processes.

METHODS

We made new textural observations of pumice lapilli from four silicic sub-Plinian and Plinian eruptions at Medicine Lake volcano (California, USA; 1060 CE Glass Mountain eruption; Heiken, 1978), Newberry volcano (Oregon, USA; 700 CE Big Obsidian Flow eruption; Kuehn, 2002), and Mount Mazama–Giiwas (Oregon; ca. 5750 BCE Cleetwood and climactic eruptions; Young, 1990; Bacon, 1983). These explosive eruptions ejected ~ 0.1 km³ (explosive phase of the Big Obsidian Flow and Glass Mountain eruptions) to ~ 60 km³ (climactic phase of the ca. 5750 BCE eruption of Mount Mazama–Giiwas) of crystal-poor rhyodacitic to rhyolitic magma. For each eruption, 100 juvenile pumice lapilli, collected from a single bed, were analyzed for their size and porosity (bulk and connected; see the Supplemental Material¹). In all suites, some pyroclasts exhibit distinct surficial textures from inter-clast amalgamation,

*E-mail: tgiachet@uoregon.edu

¹Supplemental Material. Additional information on (1) the four eruptions studied and sample collection, (2) lapilli selection, (3) measurements of volume and porosity, (4) analysis by X-Ray computed tomography and scanning electron microscopy, and (5) calculation of protopyroclasts size distributions. Please visit <https://doi.org/10.1130/G48902.1> to access the supplemental material, and contact editing@geosociety.org with any questions.

CITATION: Giachetti, T., et al., 2021, The products of primary magma fragmentation finally revealed by pumice agglomerates: *Geology*, v. 49, p. 1307–1311, <https://doi.org/10.1130/G48902.1>

visible under stereo microscope. The proportion of these clasts was determined, and 28 variably textured lapilli, wherein six to nine (some exhibiting amalgamation-like textures, some not) were arbitrarily chosen from each suite, were then analyzed by X-ray computed tomography (CT; see the Supplemental Material).

POROSITY AND EXTERNAL TEXTURE OF THE LAPILLI SUITES

The bulk porosity and the ratio of connected to bulk porosity (connectivity) of the pyroclasts suites are roughly positively correlated (Fig. 1). Moreover, median bulk porosity and connectivity increase with erupted volume and mass discharge rate, from $72\% \pm 7\%$ and 0.88 ± 0.06 , respectively, for Medicine Lake, to $76\% \pm 4\%$ and 0.89 ± 0.04 for Newberry, to $83\% \pm 4\%$ and 0.94 ± 0.03 for the Cleetwood phase of Mazama and $87\% \pm 3\%$ and 1.00 ± 0.03 for the climactic phase of the Mazama eruption. The bulk porosity and connectivity of all four suites of pyroclasts are typical of sub-Plinian and Plinian lapilli in general (Mueller et al., 2011; Colombier et al., 2017). All suites contain pumice lapilli that have surficial textural evidence of amalgamation. The presence of such

textures does not depend on the size, porosity, or connectivity of the pyroclast (Fig. 1). However, the overall proportion of extremely likely to most likely amalgamated clasts (see the Supplemental Material for details) decreases with erupted volume and mass discharge rate, from 17%–37% in the Medicine Lake and 17%–39% in the Newberry suites to 14%–25% in the Cleetwood phase and 5%–19% in the climactic phase of Mazama.

IDENTIFYING PROTOPYROCLASTS

All visually amalgamated pyroclasts, and more than a third (5 of 14) of those appearing texturally homogeneous, consist of juxtaposed domains with variable porosities, vesicle sizes, and vesicle orientations when viewed under CT (Fig. 2). These domains range in size from a few microns to >1 cm. The contrast in porosity and/or vesicle sizes and orientations between textural domains is typically sharp (Figs. 2A and 2D), but more subtle differences in vesicle texture between domains exist and are trackable in three-dimensional CT scans (e.g., Figs. 2B and 2C). Single pyroclasts can contain several to thousands of discrete domains (Fig. 2). Most domains <~30 microns are almost entirely

dense (Figs. 2E and 2F). Boundaries between some larger domains form tomographically bright bands a few microns to tens of microns in thickness (Figs. 2A and 2D). Scanning electron microscope (SEM) images taken at higher resolution show that these boundaries include partly sintered ash in between domains (Figs. 2E and 2F) and/or densified domain rims between which some pores are flattened (Fig. 2D). We note that in most CT scans, boundaries between domains are more easily identifiable toward the outskirts of the clast.

Using SEM and CT image analysis, we manually delineated textural domains from four pumice lapilli (two from Newberry, two from Medicine Lake; Figs. 3A and 3B) for which the boundaries between domains are clear enough at all sizes for these domains to be separated on the images. Although contrasting textural domains are apparent on the CT images of the Mazama pyroclasts (Figs. 2B and 2D), exact boundaries are too diffuse to delineate without significant bias; as such, the exercise was not carried out for these pyroclasts.

The new imagery allows us to quantify the size distribution of textural domains from ~3 μm up to the size of the lapilli themselves (11–31 mm). In all four cases, the size distribution of textural domains defines a power-law distribution that is best fitted using an exponent of 2.4–2.6 (Fig. 3C). Prior to amalgamation, these textural domains had a size distribution that matched that predicted by fragmentation experiments conducted on a variety of geological objects (fractal dimension of 2.5 ± 0.3 ; Turcotte, 1997; Kaminski and Jaupart, 1998).

Porous volcanic pyroclasts, when rapidly decompressed in a shock-tube apparatus, fragment if the change in pressure exceeds a threshold of approximately σ/ϕ , where $\sigma \approx 1$ MPa is the tensile strength of the silicate melt and ϕ is the porosity of the magma (Spieler et al., 2004). The fractal dimension of these products typically falls within a narrow range of 2.4 ± 0.2 (Alidibirov and Dingwell, 1996; Kueppers et al., 2006). We thus interpret the textural domains highlighted in Figure 2 to be protopyroclasts, the direct products of primary magmatic fragmentation in the conduit. Because their porosity and connectivity are typical of sub-Plinian and Plinian pumice lapilli (Fig. 1; Rust and Cashman, 2011; Colombier et al., 2017) and none of the 400 clasts analyzed have obsidian edges, amalgamated pyroclasts are highly unlikely to derive from tuffisitic infill. Instead, we posit that these protopyroclasts were preserved by amalgamation and partial sintering inside the conduit during and/or immediately following primary fragmentation (Fig. 4). The size distributions of silicic Plinian fallout deposits, which have a fractal dimension of 3.4 ± 0.3 (Fig. 3C; Kaminski and Jaupart, 1998; Rust and Cashman, 2011; Pioli et al., 2019; Carazzo et al., 2020), must

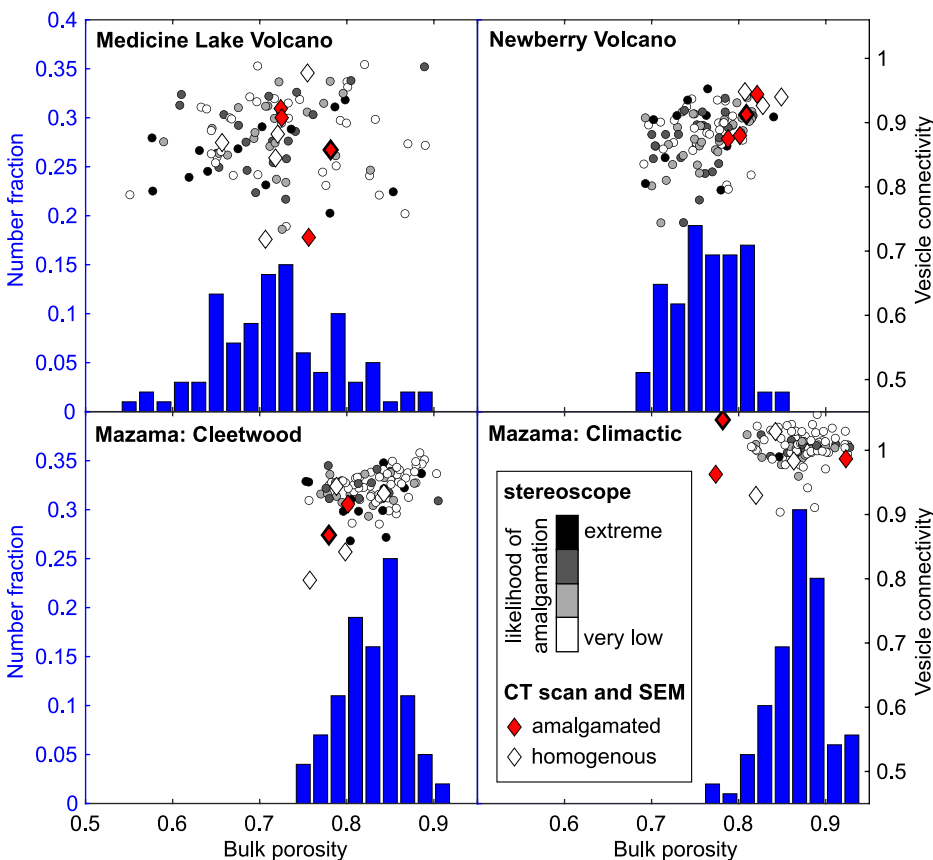


Figure 1. Pyroclast bulk porosity distribution (left axes) and ratio of connected to bulk porosity (i.e., connectivity; right axes) for each studied eruption. Circle color represents likelihood that each pyroclast is amalgamation of protopyroclasts as based on observation under stereo microscope. For clasts analyzed by X-ray computed tomography (CT) (diamonds), color indicates whether clast exhibits CT/SEM (scanning electron microscope) evidence of amalgamation. Red diamond with thicker edge corresponds to clast shown in Figure 2 for each eruption.

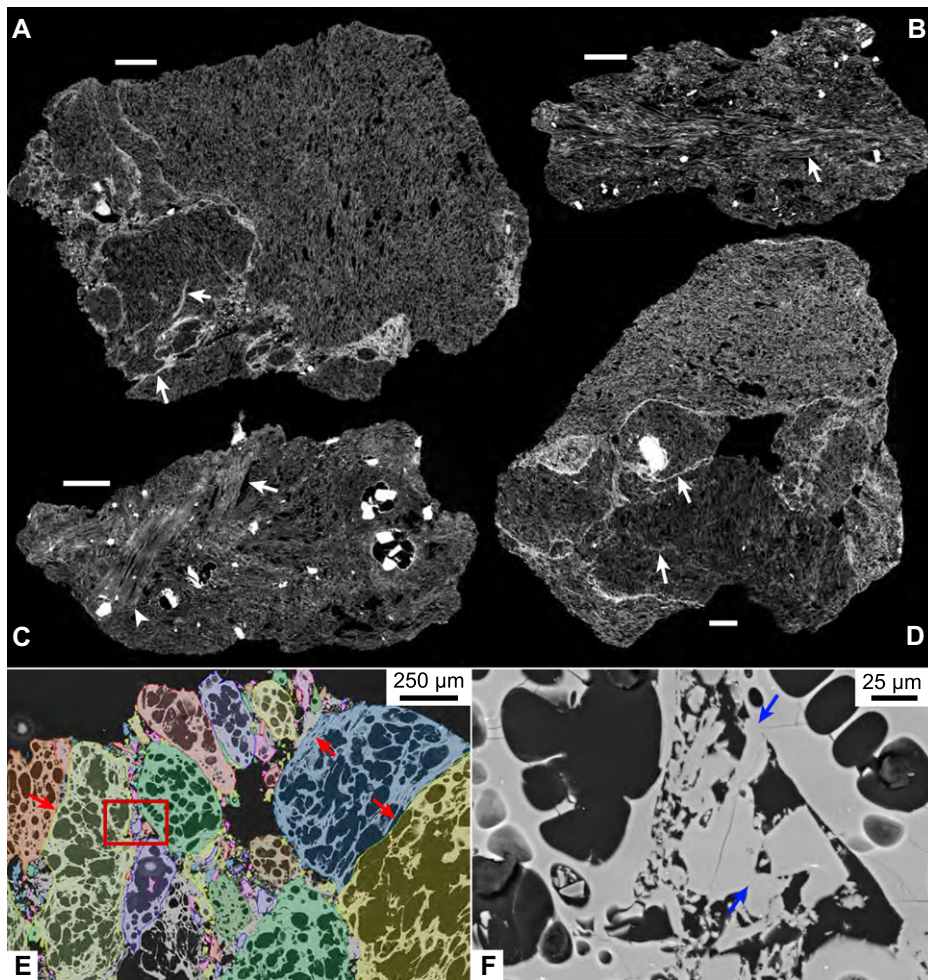


Figure 2. (A–D) Slices taken in X-ray computed tomography stacks of pumice lapilli from Newberry volcano (Oregon, USA; clast 6) (A), Cleetwood eruption of Mount Mazama (Oregon; clast 11) (B), climactic eruption of Mount Mazama (clast 4) (C), and Medicine Lake volcano (California, USA; clast 86D) (D). White arrows highlight selected boundaries between textural domains, some of which appear more subdued, usually closer to center of clasts. White scale bar is 2 mm. (E,F) Scanning electron microscope images of sample from Medicine Lake volcano (clast 8) showing partly sintered particles. Red rectangle in E shows location of F. In E, red arrows indicate flattened voids in rim of individual protopyroclasts. All easily identifiable protopyroclasts have been colored for easier visualization only. In F, blue arrows point to examples of partly sintered ash particles.

thus be largely overprinted by amalgamation and by secondary fragmentation in the conduit and the plume, and so can only give limited insight into primary magmatic fragmentation. The number density of protopyroclasts $>1 \mu\text{m}$ in the four pumice lapilli analyzed is $\sim 10^{15} \text{ m}^{-3}$ of magma (Fig. 2C), nearly an order of magnitude less than the number density of pyroclasts $>1 \mu\text{m}$ ultimately produced by Plinian eruptions (Rust and Cashman, 2011). This discrepancy likely arises from secondary fragmentation augmenting the production of smaller pyroclasts in the conduit and plume.

SINTERING OF PROTOPYROCLASTS

For protopyroclasts to amalgamate, they must collide at low-enough energies to not further break apart and stick together (Dufek et al., 2012). We posit that this occurs during the flu-

idization of the packed beds of pyroclasts. This is a zone between the unfragmented magma below and the fully fluidized gas-pyroclast mixture above—in other words, at or just above the fragmentation zone (Darteville and Valentine, 2007). In that zone, both the density of particles and their acceleration are high, but acceleration slightly differs for particles of different size, promoting low-energy collisions. As melt viscosity increases during ascent post-fragmentation due to permeable outgassing and diffusive water loss (Rust and Cashman, 2011), so too does the sintering time scale. Pyroclasts thus have the highest chance to collide, amalgamate, and partially sinter in the vicinity of the fragmentation zone. Obsidian pyroclasts from the 1340 CE North Mono eruption (Mono Craters, California) formed by cycles of fragmentation, sintering and/or suturing, and annealing and/or

relaxation over varying depths on the conduit wall (Gardner et al., 2017; Watkins et al., 2017). We propose that this process also occurs inside the gas-pyroclast mixture across the conduit, wherein limited residence time during rapid final ascent limits maturation and densification of the aggregates, preserving protopyroclasts' initial sizes and textures.

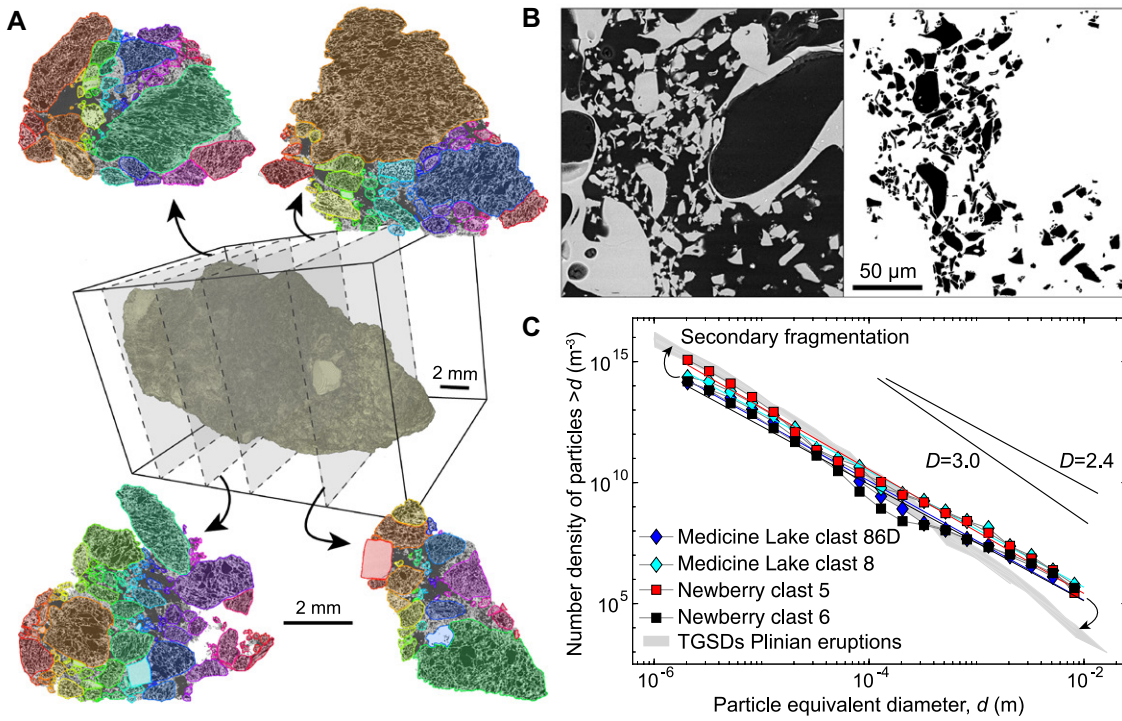
Sintering after initial amalgamation must rapidly occur between fragmentation and quench, over the course of ~ 10 – 60 s (Gardner et al., 1996). In the absence of confining pressure, the sintering time scale of randomly packed, monodisperse spherical particles is given by (Wadsworth et al., 2019):

$$\tau \approx \frac{\mu R}{\sigma}, \quad (1)$$

where τ (in seconds) is the sintering time scale, μ (in Pa·s) is the viscosity of the melt, R (in meters) is the particle radius, and σ is the surface tension. Sintering between protopyroclasts appears limited, usually occurring over length scales of $\sim 10^{-5}$ m or less (Figs. 2E and 2F). Assuming disequilibrium degassing, rhyolitic melt viscosity at fragmentation is $\sim 10^6$ Pa·s (Gonnermann and Houghton, 2012; Hajimirza et al., 2021), a reasonable value for a wide range of silicic magmas (Gardner et al., 1996). For a surface tension of ~ 0.2 N/m (Bagdassarov et al., 2000) and in the absence of confining pressure, $R = \sim 10^{-5}$ m protopyroclasts can sinter above the fragmentation zone within ~ 50 s, prior to quench (Equation 1).

IMPLICATIONS

We examined typical pyroclasts from four sub-Plinian and Plinian eruptions that span more than three orders of magnitude of erupted ejecta by volume and more than two orders of magnitude of mass discharge rates. We postulate that syn- and/or post-fragmentation amalgamation and partial sintering of protopyroclasts in the conduit is widespread and has been previously overlooked or interpreted differently. Highly silicic pumice-fall agglomerates have been rarely reported (Newberry, Oregon, USA; Kuehn, 2002; and Santorini, Greece; Taddeucci and Wohletz, 2001), yet contiguous heterogeneous textures at the sub-millimeter scale have been widely documented in highly silicic tephra (e.g., Wright and Weinberg, 2009, their figures 1A and 4A; Schipper et al., 2013, their figure 9; Pistolesi et al., 2015, their figure 15). While they are usually interpreted as resulting from heterogeneities in material properties and/or localized degassing, these textures may be from syn- and/or post-fragmentation amalgamation and partial sintering of protopyroclasts, as described herein. Additionally, Newberry ($\sim 10^7$ kg/s; Gardner et al., 1998) and Medicine Lake pyroclasts preserve these textures more often and more distinctly than do those from Mazama



using a power-law distribution $N = \lambda d^{-D}$ (where N is the number of particles greater than size d , λ is a scaling factor, and D is the power-law exponent), give $D = 3.0-3.3$, whereas protopyroclast size distributions are best fit with $D = 2.4-2.6$ (2.40 and 2.56 for Newberry clast 6 and clast 5, respectively; 2.40 and 2.47 for Medicine Lake clast 8 and clast 86D). The two black reference lines illustrate the difference in slope between power-law distributions with fractal dimension of 2.4 and 3.0.

(10^8-10^9 kg/s; Young, 1990). This observation could be an indication that the fluidization of packed beds of protopyroclasts at fragmentation during more explosive eruptions is more efficient, leaving less time for mixing and amal-

gamation of protopyroclasts with highly contrasting textures.

Magmatic fragmentation converts potential energy from the compressed gas inside bubbles into kinetic energy and surface energy of fractures

in the melt (Grady, 1982). The size distribution of fragmentation products should reflect eruption explosivity, wherein the fractal dimension of the fragment size distribution increases with the potential energy for fragmentation (Kueppers et al.,

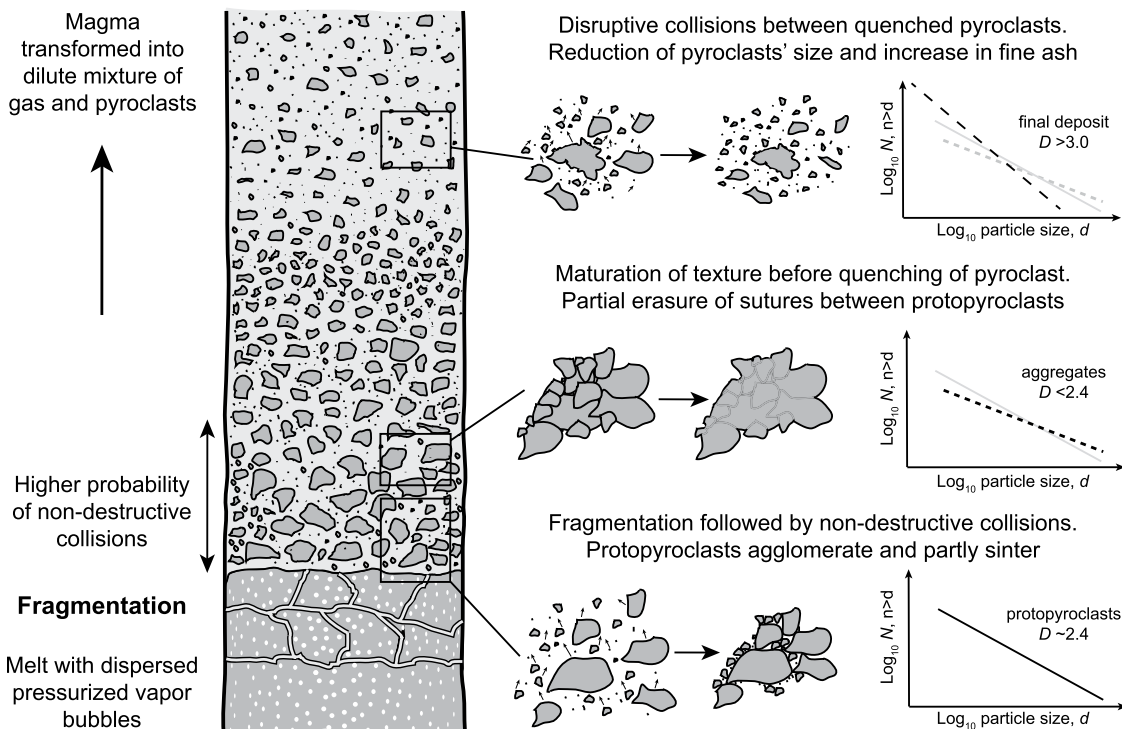


Figure 4. Diagram illustrating primary and secondary fragmentation processes occurring within the conduit and their effects on pyroclast grain-size distributions. Diagram is not to scale; slopes on graphs have been exaggerated to highlight evolution of particle size distribution.

2006). However, the unconstrained overprint of secondary fragmentation on the final size distribution of tephra renders this task challenging. The textures described here provide a framework for quantifying the size distribution of primary magmatic fragmentation products, and so could be used to obtain the potential energy for fragmentation (Yew and Taylor, 1994; Kolzenburg et al., 2013). These textures also show that, contrary to what is claimed at this time, studies of the size and texture of the final pyroclasts (rather than individual protopyroclasts) may tell a post- rather than pre-fragmentation story.

ACKNOWLEDGMENTS

We thank L. Gurioli, U. Kueppers, and C. Rengli for their thorough review of the manuscript, and J. Schmith and E. Johnson for their comments on an earlier version. We also thank M. Norman for his efficient handling of our manuscript. We also are grateful to J. Dufek, H.M. Gonnermann, S. Hajimirza, and F. Wadsworth for insightful discussions that helped shape the study. T. Giachetti, K. Trafton, and J. Watkins were partly funded by U.S. National Science Foundation grant EAR-2024510. J. Gardner was partly funded by U.S. National Science Foundation grant EAR-1725186. Any use of trade, firm, or product names is for descriptive purposes only and does not imply endorsement by the U.S. Government.

REFERENCES CITED

Alidibirov, M., and Dingwell, D.B., 1996, Magma fragmentation by rapid decompression: *Nature*, v. 380, p. 146–148, <https://doi.org/10.1038/380146a0>.

Bacon, C.R., 1983, Eruptive history of Mount Mazama and Crater Lake caldera, Cascade Range, USA: *Journal of Volcanology and Geothermal Research*, v. 18, p. 57–115, [https://doi.org/10.1016/0377-0273\(83\)90004-5](https://doi.org/10.1016/0377-0273(83)90004-5).

Bagdassarov, N., Dorfman, A., and Dingwell, D.B., 2000, Effect of alkalis, phosphorus, and water on the surface tension of haplogranite melt: *American Mineralogist*, v. 85, p. 33–40, <https://doi.org/10.2138/am-2000-0105>.

Carazzo, G., Tait, S., Michaud-Dubuy, A., Fries, A., and Kaminski, E., 2020, Transition from stable column to partial collapse during the 79 cal CE P3 Plinian eruption of Mt. Pelée volcano (Lesser Antilles): *Journal of Volcanology and Geothermal Research*, v. 392, 106764, <https://doi.org/10.1016/j.jvolgeores.2019.106764>.

Colombier, M., Wadsworth, F.B., Gurioli, L., Scheu, B., Kueppers, U., Di Muro, A., and Dingwell, D.B., 2017, The evolution of pore connectivity in volcanic rocks: *Earth and Planetary Science Letters*, v. 462, p. 99–109, <https://doi.org/10.1016/j.epsl.2017.01.011>.

Dartevelle, S., and Valentine, G.A., 2007, Transient multiphase processes during the explosive eruption of basalt through a geothermal borehole (Námafjall, Iceland, 1977) and implications for natural volcanic flows: *Earth and Planetary Science Letters*, v. 262, p. 363–384, <https://doi.org/10.1016/j.epsl.2007.07.053>.

Dingwell, D.B., 1996, Volcanic dilemma—Flow or blow?: *Science*, v. 273, p. 1054–1055, <https://doi.org/10.1126/science.273.5278.1054>.

Dufek, J., Manga, M., and Patel, A., 2012, Granular disruption during explosive volcanic eruptions: *Nature Geoscience*, v. 5, p. 561–564, <https://doi.org/10.1038/ngeo1524>.

Gardner, J.E., Thomas, R.M., Jaupart, C., and Tait, S., 1996, Fragmentation of magma during Plinian volcanic eruptions: *Bulletin of Volcanology*, v. 58, p. 144–162, <https://doi.org/10.1007/s004450050132>.

Gardner, J.E., Carey, S., and Sigurdsson, H., 1998, Plinian eruptions at Glacier Peak and Newberry volcanoes, United States: Implications for volcanic hazards in the Cascade Range: *Geological Society of America Bulletin*, v. 110, p. 173–187.

Gardner, J.E., Llewellyn, E.W., Watkins, J.M., and Befus, K.S., 2017, Formation of obsidian pyroclasts by sintering of ash particles in the volcanic conduit: *Earth and Planetary Science Letters*, v. 459, p. 252–263, <https://doi.org/10.1016/j.epsl.2016.11.037>.

Gonnermann, H.M., and Houghton, B.F., 2012, Magma degassing during the Plinian eruption of Novarupta, Alaska, 1912: *Geochemistry Geophysics Geosystems*, v. 13, Q10009, <https://doi.org/10.1029/2012GC004273>.

Gonnermann, H.M., and Manga, M., 2007, The fluid mechanics inside a volcano: *Annual Review of Fluid Mechanics*, v. 39, p. 321–356, <https://doi.org/10.1146/annurev.fluid.39.050905.110207>.

Grady, D.E., 1982, Local inertial effects in dynamic fragmentation: *Journal of Applied Physics*, v. 53, p. 322–325, <https://doi.org/10.1063/1.329934>.

Hajimirza, S., Gonnermann, H.M., and Gardner, J.E., 2021, Reconciling bubble nucleation in explosive eruptions with geospeedometers: *Nature Communications*, v. 12, p. 1–8, <https://doi.org/10.1038/s41467-020-20541-1>.

Heiken, G., 1978, Plinian-type eruptions in the Medicine Lake Highland, California, and the nature of the underlying magma: *Journal of Volcanology and Geothermal Research*, v. 4, p. 375–402, [https://doi.org/10.1016/0377-0273\(78\)90023-9](https://doi.org/10.1016/0377-0273(78)90023-9).

Jones, T.J., Russell, J.K., Lim, C.J., Ellis, N., and Grace, J.R., 2017, Pumice attrition in an air-jet: *Powder Technology*, v. 308, p. 298–305, <https://doi.org/10.1016/j.powtec.2016.11.051>.

Kaminski, E., and Jaupart, C., 1998, The size distribution of pyroclasts and the fragmentation sequence in explosive volcanic eruptions: *Journal of Geophysical Research*, v. 103, p. 29,759–29,779, <https://doi.org/10.1029/98JB02795>.

Kolzenburg, S., Russell, J.K., and Kennedy, L.A., 2013, Energetics of glass fragmentation: Experiments on synthetic and natural glasses: *Geochemistry Geophysics Geosystems*, v. 14, p. 4936–4951, <https://doi.org/10.1002/2013GC004819>.

Kuehn, S.C., 2002, Stratigraphy, distribution, and geochemistry of the Newberry Volcano tephra [Ph.D. thesis]: Pullman, Washington, Washington State University, 701 p.

Kueppers, U., Perugini, D., and Dingwell, D.B., 2006, “Explosive energy” during volcanic eruptions from fractal analysis of pyroclasts: *Earth and Planetary Science Letters*, v. 248, p. 800–807, <https://doi.org/10.1016/j.epsl.2006.06.033>.

Mueller, S., Scheu, B., Kueppers, U., Spieler, O., Richard, D., and Dingwell, D.B., 2011, The porosity of pyroclasts as an indicator of volcanic explosivity: *Journal of Volcanology and Geothermal Research*, v. 203, p. 168–174, <https://doi.org/10.1016/j.jvolgeores.2011.04.006>.

Papale, P., 1999, Strain-induced magma fragmentation in explosive eruptions: *Nature*, v. 397, p. 425–428, <https://doi.org/10.1038/17109>.

Pioli, L., Bonadonna, C., and Pistolesi, M., 2019, Reliability of total grain-size distribution of tephra deposits: *Scientific Reports*, v. 9, 10006, <https://doi.org/10.1038/s41598-019-46125-8>.

Pistolesi, M., Cioni, R., Bonadonna, C., Elissondo, M., Baumann, V., Bertagnini, A., Chiari, L., Gonzales, R., Rosi, M., and Francalanci, L., 2015, Complex dynamics of small-moderate volcanic events: The example of the 2011 rhyolitic Cordón Caulle eruption, Chile: *Bulletin of Volcanology*, v. 77, p. 3–24, <https://doi.org/10.1007/s00445-014-0898-3>.

Rust, A.C., and Cashman, K.V., 2011, Permeability controls on expansion and size distributions of pyroclasts: *Journal of Geophysical Research*, v. 116, B11202, <https://doi.org/10.1029/2011JB008494>.

Schipper, C.I., Castro, J.M., Tuffen, H., James, M.R., and How, P., 2013, Shallow vent architecture during hybrid explosive-effusive activity at Cordón Caulle (Chile, 2011–12): Evidence from direct observations and pyroclast textures: *Journal of Volcanology and Geothermal Research*, v. 262, p. 25–37, <https://doi.org/10.1016/j.jvolgeores.2013.06.005>.

Spieler, O., Kennedy, B., Kueppers, U., Dingwell, D.B., Scheu, B., and Taddeucci, J., 2004, The fragmentation threshold of pyroclastic rocks: *Earth and Planetary Science Letters*, v. 226, p. 139–148, <https://doi.org/10.1016/j.epsl.2004.07.016>.

Taddeucci, J., and Wohletz, K.H., 2001, Temporal evolution of the Minoan eruption (Santorini, Greece), as recorded by its Plinian fall deposit and inter-layered ash flow beds: *Journal of Volcanology and Geothermal Research*, v. 109, p. 299–317, [https://doi.org/10.1016/S0377-0273\(01\)00197-4](https://doi.org/10.1016/S0377-0273(01)00197-4).

Turcotte, D.L., 1997, *Fractals and Chaos in Geology and Geophysics* (second edition): Cambridge, UK, Cambridge University Press, 398 p., <https://doi.org/10.1017/CBO9781139174695>.

Wadsworth, F.B., et al., 2019, A general model for welding of ash particles in volcanic systems validated using in situ X-ray tomography: *Earth and Planetary Science Letters*, v. 525, 115726, <https://doi.org/10.1016/j.epsl.2019.115726>.

Watkins, J.M., Gardner, J.E., and Befus, K.S., 2017, Nonequilibrium degassing, regassing, and vapor fluxing in magmatic feeder systems: *Geology*, v. 45, p. 183–186, <https://doi.org/10.1130/G38501.1>.

Wright, H.M., and Weinberg, R.F., 2009, Strain localization in vesicular magma: Implications for rheology and fragmentation: *Geology*, v. 37, p. 1023–1026, <https://doi.org/10.1130/G30199A.1>.

Yew, C.H., and Taylor, P.A., 1994, A thermodynamic theory of dynamic fragmentation: *International Journal of Impact Engineering*, v. 15, p. 385–394, [https://doi.org/10.1016/0734-743X\(94\)80023-3](https://doi.org/10.1016/0734-743X(94)80023-3).

Young, S.R., 1990, *Physical volcanology of Holocene airfall deposits from Mt Mazama, Crater Lake, Oregon* [Ph.D. thesis]: Lancaster, UK, University of Lancaster, 298 p.

Zhang, Y., 1999, A criterion for the fragmentation of bubbly magma based on brittle failure theory: *Nature*, v. 402, p. 648–650, <https://doi.org/10.1038/45210>.

Printed in USA